Modeling Spray Pyrolysis Deposition

Lado Filipovic, *Member, IAENG*, Siegfried Selberherr, Giorgio C. Mutinati, Elise Brunet, Stephan Steinhauer, Anton Köck, Jordi Teva, Jochen Kraft, Jörg Siegert, and Franz Schrank

***Abstract*—The deposition of a thin tin oxide film allows for the manufacture of modern gas sensors. Spray pyrolysis deposition is used to grow the required thin films, as it can be seamlessly integrated into a standard CMOS processing sequence. A model for spray pyrolysis deposition is developed and implemented within the Level Set framework. Two models for the topography modification due to spray pyrolysis deposition are presented, with an electric and a pressure atomizing nozzle. The resulting film growth is modeled as a layer by layer deposition of the individual droplets which reach the wafer surface or as a CVD-like process, depending on whether the droplets form a vapor near the interface or if they deposit a film only after surface collision.**

***Index Terms*—Spray pyrolysis deposition, Tin oxide film, Topography simulation, Level Set, Smart gas sensors**

I. Introduction

The spray pyrolysis deposition technique is gaining traction in the scientific community due to its cost effectiveness and ease of integration into a standard CMOS process. The technique is used to grow crystal powders [1], which can then be further annealed for use for gas sensors, solar cells, and other applications.

A. Tin-Oxide Based Gas Sensors

Among many gas sensing materials, tin oxide (SnO_2) has proved to have a high potential for smart gas sensing devices and many SnO_2-based devices have already been realized [2]. The growth of the ultrathin SnO_2 layers on semiconductor structures requires for a deposition step which can easily be integrated into the traditional CMOS process [3]. The main concern with today's gas sensor devices are their bulky nature, high power consumption, and complex manufacturing techniques which do not allow for easy integration with CMOS processing steps.

A sensor which uses films with thicknesses of 50nm and 100nm has already been reported in [2]. The sensor itself operates on a microsized hot plate which heats the sensor locally to 250–400^{o}C in order to detect humidity and carbon monoxide in the environment, down to a concentration of under 5ppm. The sensing mechanism of SnO_2 is related to the ionosorption of gas species over the surface, leading to charge transfer between the gas and surface molecules and changes in the electrical conductance [2].

Manuscript submitted March 05, 2013; revised April 3, 2013. This work has been partly performed in the COCOA-CATRENE European project and in the project ESiP. In this latter the Austrian partners are funded by the national funding institution for applied research and development in Austria, the Austrian Research Promotion Agency (FFG) under project no. 824954 and the ENIAC Joint Undertaking. The work has also been partly performed in the Christian Doppler Laboratory for Reliability Issues in Microelectronics at the Institute for Microelectronic.

L. Filipovic and S. Selberherr are with the Institute for Microelectronics, TU Wien, Gußhausstraße 27–29/E360, A-1040 Wien, Austria (Phone: +43-1-58801-36036, Fax: +43-1-58801-36099, e-mail: filipovic|selberherr@iue.tuwien.ac.at).

G. C. Mutinati, E. Brunet, S. Steinhauer, and A. Köck are with Molecular Diagnostics, Health & Environment, AIT GmbH, Donau-City-Straße 1, A-1220 Wien, Austria (e-mail: Giorgio.Mutinati|Elise.Brunet.fl|Stephan.Steinhauer.fl|Anton.Koeck@ait.ac.at).

J. Teva, J. Kraft, J. Siegert, and F. Schrank are with ams AG, Tobelbaderstrasse 30, A-8141 Unterpremstaetten, Austria (e-mail: Jordi.Teva|Jochen.Kraft|Joerg.Siegert|Franz.Schrank@ams.com)

B. Level Set Method

The presented simulations and models function fully within the process simulator presented in [4]. The Level Set method is utilized in order to describe the top surface of a semiconductor wafer as well as the interfaces between different materials. The Level Set method describes a movable surface $\mathcal{S}(t)$ as the zero Level Set of a continuous function $\Phi(\vec{x},t)$ defined on the entire simulation domain,

$$\mathcal{S}(t) = \{\vec{x} : \Phi(\vec{x},t) = 0\}. \tag{1}$$

The continuous function $\Phi(\vec{x},t)$ is obtained using a signed distance transform

$$\Phi(\vec{x},t=0) := \begin{cases} -\min\limits_{\vec{x}' \in \mathcal{S}(t=0)} \|\vec{x}-\vec{x}'\| & \text{if } \vec{x} \in \mathcal{M}(t=0) \\ +\min\limits_{\vec{x}' \in \mathcal{S}(t=0)} \|\vec{x}-\vec{x}'\| & \text{else,} \end{cases} \tag{2}$$

where $\mathcal{M}$ is the material described by the Level Set surface $\Phi(\vec{x},t=0)$. The implicitly defined surface $\mathcal{S}(t)$ describes a surface evolution, driven by a scalar velocity $V(\vec{x})$, using the Level Set equation

$$\frac{\partial \Phi}{\partial t} + V(\vec{x}) \|\nabla \Phi\| = 0. \tag{3}$$

In order to find the location of the evolved surface, the velocity field $V(\vec{x})$, which is a calculated scalar value, must be found.

C. Spray Pyrolysis Deposition

During the last several decades, coating technologies have garnered considerable attention, mainly due to their functional advantages over bulk materials, processing flexibility, and cost considerations [5]. Thin film coatings may be deposited using physical methods or chemical methods. Spray pyrolysis is a technique which uses a liquid source for thin film coating.

The main advantages of spray pyrolysis over other similar techniques are:
- Seamless incorporation in a standard CMOS process.
- Cost effectiveness.
- Substrates with complex geometries can be coated.
- Relatively uniform and high quality coatings.
- No high temperatures are required during processing.

The spray pyrolysis process is used for the deposition of a transparent layer on glass [6], the deposition of a SnO_2

ISBN: 978-988-19252-8-2
ISSN: 2078-0958 (Print); ISSN: 2078-0966 (Online)

layer for gas sensor applications [7], the deposition of a YSZ layer for solar cell applications [8], anodes for lithium-ion batteries [9], and optoelectronic devices [10].

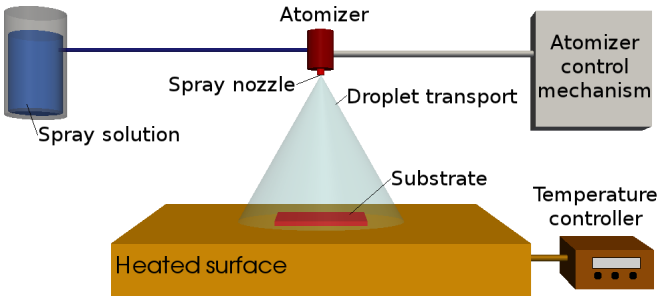

Fig. 1. General schematic of a spray pyrolysis deposition process.

The general simplified scheme for spray pyrolysis deposition is shown in Fig. 1, where three processing steps can be viewed and analyzed:

1) Atomization of the precursor solution.
2) Aerosol transport of the droplet.
3) Decomposition of the precursor to initiate film growth

II. Process Sequence During Deposition

A. Precursor Atomization

The atomization procedure is the first step in the spray pyrolysis deposition system. The idea is to generate droplets from a spray solution and send them, with some initial velocity, towards the substrate surface. Spray pyrolysis normally uses air blast, ultrasonic, or electrostatic techniques [11]. The atomizers differ in resulting droplet size, rate of atomization, and the initial velocity of the droplets. It has been shown that the size of the generated droplet is not related to any fluid property of the precursor solution and depends solely on the fluid charge density level ρ_e as shown in [12]

$$r^2 = \left(\frac{-\alpha'}{\beta'} \right) \frac{3\epsilon_0}{q\rho_e}, \tag{4}$$

where ϵ_0 is the permittivity, q is the elementary charge, and $-\alpha'/\beta'$ is a constant value equal to $\sim 1.0 \times 10^{-17}$J. The mass of a droplet, assuming a spherical shape depends on its density

$$m = \frac{4\pi}{3} \rho_q r^3, \tag{5}$$

where r is the droplet radius and ρ_q is the droplet density. The initial leaving velocity of the droplet is an important parameter as it determines the rate at which the droplets reach the substrate surface, the heating rate of the droplet, and the amount of time the droplet remains in transport

Due to its ease of production, many companies chose to use pressure atomizers instead of the ultrasonic atomizers. Therefore, this work will mainly concern itself with the pressure and electrostatic atomizers, characterized in further detail in [7], [11], respectively.

A pressure, or air blast, atomizer uses high speed air in order to generate an aerosol from a precursor solution. Increasing the air pressure causes a direct decrease in the generated mean droplet diameter. Inversely, increasing the liquid pressure causes a direct increase in the mean droplet diameter [13]. Perednis [11] showed that all droplets sprayed from an air blast atomizer are contained within a 70^o spray cone angle, while half are within a narrower 12^o angle. It was also determined that the flow rate has a very small influence on the spray characteristics, which can be mostly ignored for modeling.

B. Aerosol Transport of Droplets

After the droplet leaves the atomizer, it travels through the ambient with an initial velocity determined by the atomizer. In the aerosol form, the droplets are transported with the aim of as many droplets as possible reaching the surface. As the droplets move through the ambient, they experience physical and chemical changes depicted in Fig. 2.

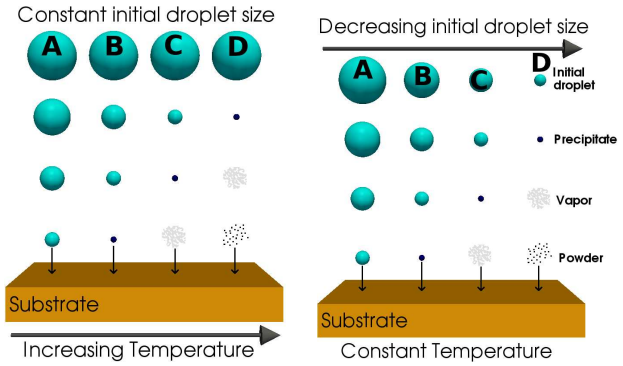

Fig. 2. Spray pyrolysis droplets modifying as they are transported from the atomizing nozzle to the substrate. Whether the temperature [14] or the initial droplet size [15] are varied, there are four potential paths which the droplet can take as it moves towards the substrate (A-D).

As the droplet traverses the ambient, there are four forces simultaneously acting on it, describing its path. Those forces are gravitational, electrical, thermophoretic, and the Stokes force. As shown in Fig. 2, the droplets experience evaporation during their flight, which affects the influence of the forces on their trajectory. Some experimental results from [16] indicate that solid particles could form, when the reactor temperature is low, when the precursor solution concentration is high, and when the flow rate of the carrier gas (N_2) is low.

1) Gravitational force: The gravitational force is the force pulling the droplet downward. The size of the force depends on the mass of the traveling droplet, given by (5). For small droplets the force of gravity is too small to allow it to arrive at the surface before it is fully evaporated. For larger particles, the force of gravity is the driving force behind the droplet transport.

2) Electrical force: The electrical force is applicable to spray pyrolysis systems which include an additional electrical source governing the droplet's trajectory. When an air blast atomizer is used, high speed air is the cause of atomization and aerosol production. Ultrasonic atomizers are electrically driven, whereby an electric generator is vibrated at ultrasonic frequencies through a titanium nozzle. Increasing the frequency can result in smaller droplet sizes. Electric spray deposition (ESD) atomizers use a strong electric field at the liquid-gas interface to generate charged droplets. Therefore, air blast atomizers do not have additional contributions from an electrical force and the droplet transport is driven by the gravitational force and the initial velocity, while for spray pyrolysis deposition using ultrasonic and ESD atomizers,

ISBN: 978-988-19252-8-2
ISSN: 2078-0958 (Print); ISSN: 2078-0966 (Online)

the electrical force is the main component which drives the droplets downwards. The electrical force acting on a droplet is usually several orders of magnitude larger than the gravitational force [8] and is given by

$$F_e = q_d\, E, \tag{6}$$

where E is the generated electric field strength and q_d is the droplet charge. q_d depends on the temporal change of the droplet and is given by

$$q_d = 8\,\pi\sqrt{\gamma\,\epsilon_0\,r^3}\cdot\frac{t}{t+t_0}, \qquad t_0 = \frac{4}{b\,\mathrm{div}E} \tag{7}$$

where γ is the liquid-gas surface tension, ϵ_0 is the electrical permittivity, and b is the ionic mobility [15].

3) Stokes force: The stokes force is the drag experienced by the droplet due to the air resistance in the ambient. The force is caused by the friction between the droplet and air molecules. The Stokes force is a factor of the particle's velocity and size. Therefore, large droplets which move with a high velocity will experience the largest retarding force according to

$$F_S = 6\,\pi\,\eta_a\,r\,(v_d - v_a)\left(1+\frac{3}{8}\mathrm{Re}\right), \tag{8}$$

where η_a is the viscosity of air, v_d is the droplet velocity, v_a is the air velocity, and Re is the Reynolds number.

4) Thermophoretic force: The thermophoretic force is a retarding force, causing droplets to significantly decrease their velocity as they approach the heated substrate. Fig. 3 shows the temperature distribution near a heated substrate. The results for the 210^{o}C, 250^{o}C, and 310^{o}C samples are taken from [11], while the results for the 400^{o}C sample are measured. It is evident that the air temperature increases steeply due to the forced convection cooling effect of the air flow when close to the heated substrate. Because the thermophoretic force depends on the thermal gradient in the transport environment, it can be concluded that it will have no effect on the droplet movement, when it is more than several ($\sim$5-7) mm away from the substrate. However, in this high thermal gradient region, the thermophoretic force begins to dominate. This is true for pressure spray deposition (PSD) systems where the main driving force is gravity; however, for ESD systems, the electrical force is often stronger than the thermophoretic force [11]. The increased temperature has additional effects on the droplet, such as a reduction in its size due to droplet evaporation in the region.

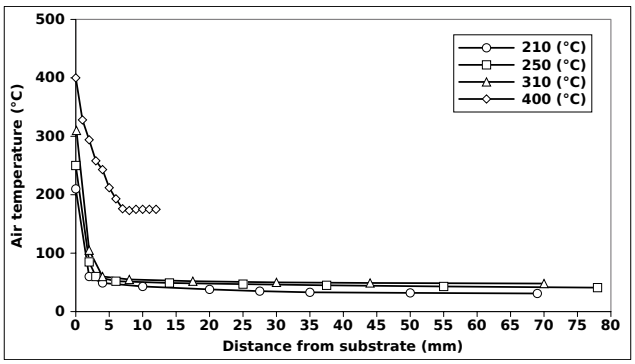

Fig. 3. Air temperature above a heated plate for substrate temperatures 210^{o}C, 250^{o}C, 310^{o}C, and 400^{o}C during a pressurized spray process.

The equation governing the strength of the thermophoretic force is given by

$$F_t = \frac{3\,\pi\,\eta_a^2\,r}{\rho_a}\cdot\frac{3\kappa_a}{2\kappa_a^2+\kappa_d}\cdot\frac{\nabla\,(T_a)}{T_a}, \tag{9}$$

where η_a is the viscosity of air, T_d is the droplet temperature, T_a is the air temperature, ρ_a is the density of the air, and κ_a and κ_d are the thermal conductivities of the air and the droplet, respectively. It should be mentioned that (9) is only valid for droplets whose radius is much larger than the mean free path of the air molecules.

C. Precursor Decomposition

The precursor, as it moves through the heated ambient undergoes various changes, which are characterized in Fig. 2. Evaporation, precipitate formation, and vaporization all occur depending on the droplet size and ambient temperature. Fig. 2 shows the four physical forms in which the droplet may interact with the substrate surface. Although all processes occur during deposition, process C, the CVD-like deposition is desired to yield a dense high quality film [11].

When the processing environment causes droplets to evaporate prior to reaching the substrate vicinity, a precipitate will form early. As the precipitate reaches the immediate vicinity of the substrate, it is converted into a vapor state and it undergoes a heterogeneous reaction through the following steps [15]:

1) Reactant molecules diffuse to the surface.
2) Adsorption of some molecules at the surface.
3) Surface diffusion and a chemical reaction, incorporating the reactant into the lattice.
4) Desorption and diffusion of the product molecules from the surface.

This is a classical CVD reaction, which results in a high quality film deposition and a high sticking probability.

III. Modeling Droplet Transport

Forces acting on the droplet can be used in order to calculate the location where the droplet makes impact with the surface. This is a challenge because the simulation environment must now be divided into several segments. The first segment which must be treated separately is the thermal zone which is within 10mm of the wafer surface. In this area, the temperature gradient shown in Fig. 3 is high and the thermal forces play a significant role in the droplet speed as well as size, due to evaporation. In addition, when the electrical force is included, the complexity of the problem is significantly increased.

Fig. 4 shows how the simulation space is divided in order to accommodate the thermal zone for droplets. A detailed drivation of the droplet transport equations can be found in [17].

A. Effects of external forces on droplet transport

In order to follow the trajectory of a droplet after leaving the atomizer and under the influence of gravity, Stokes, electric, and thermophoretic forces, the distance required for the droplet to travel, the initial velocity v_0, and the droplet radius r_d are known. Although the thermophoretic

ISBN: 978-988-19252-8-2
ISSN: 2078-0958 (Print); ISSN: 2078-0966 (Online)

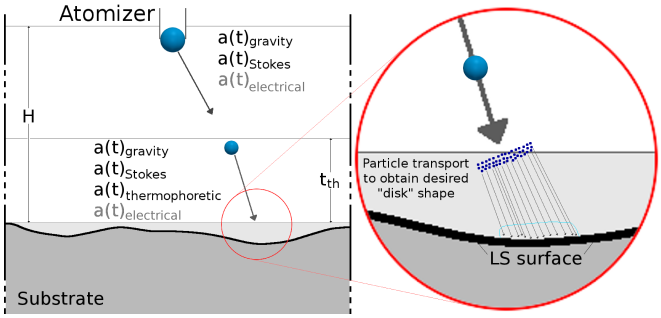

Fig. 4. The droplet transport in the space above the substrate surface and the accelerations which are considered in the transport model. T_{th} is the height of the thermal zone (∼10mm for ESD, ∼5mm for PSD), and H is the distance between the substrate and atomizer.

force does not affect the droplet motion until it reaches the vicinity of the wafer, it will be included in the derivation of the equations of motion. This allows for the most complex system to be solved, which includes all forces. Given the four forces discussed previously, the vertical acceleration experienced by the particle is given by

$$a_v(t) = g - l + s\,v_v(t) + c\,d_v(t), \tag{10}$$

where g and l are accelerations caused by the gravitational and thermophoretic forces, respectively. Acceleration s is velocity-dependent and caused by the Stokes force, while c is the linearized displacement-dependent acceleration due to the electrical force

$$l = \frac{27\,\eta_a^2\,\kappa_a\,\nabla T}{4\,\rho_a\,\rho_d\,T\,(2\kappa_a + \kappa_d)\,r_d^2}, \qquad s = \frac{9\,\eta_a}{2\,\rho_d\,r_d^2},,$$
$$c_v = \frac{6}{\rho_d}\sqrt{\frac{\gamma\,\epsilon_0}{r_d^3}}\cdot\frac{\Phi_0}{H}\cdot\frac{K_V}{\log\left(4H/R\right)}c_e, \tag{11}$$

where Φ_0 and H are the applied electrical potential and distance between the nozzle and substrate, respectively. R is the outer radius of the nozzle, while K_V is a value which ranges from 0 to 1 depending on the H/R ratio [18]. The variable c_e is a linearization constant which represents a best-fit to the electric field in the region. Fig. 5 shows the value for the normalized potential $\Phi^* = \Phi/\Phi_0$ and its distribution in an ESD deposition setup. The atomizing nozzle is located at $(0, 1)$. The inset shows the electric field distribution in the same simulation space. It is evident that the strength of the electric field is not uniform or linear, but that the field causes charged droplets to spread radially.

For the purposes of spray deposition, it is often assumed that the value of K_V is 1, because the ratio of H/R is on the order of several hundreds, which gives a value close to 1 for K_V. This value is adjusted in the model using the relationship

$$K_V = 1 - e^{-0.021\frac{H}{R}}. \tag{12}$$

In fact, assuming that $K_V = 1$ can cause erroneous results for the electric field. The negative exponential dependence on R from (12) is in the numerator of c_v in (11), which shows an additional inverse logarithmic dependence in the denominator. A plot of the fraction $K_V/\left[\log\left(4H/R\right)\right]$ for various R values is shown in Fig. 6, when the variation in K_V is taken into account and when it is assumed that $K_V = 1$.

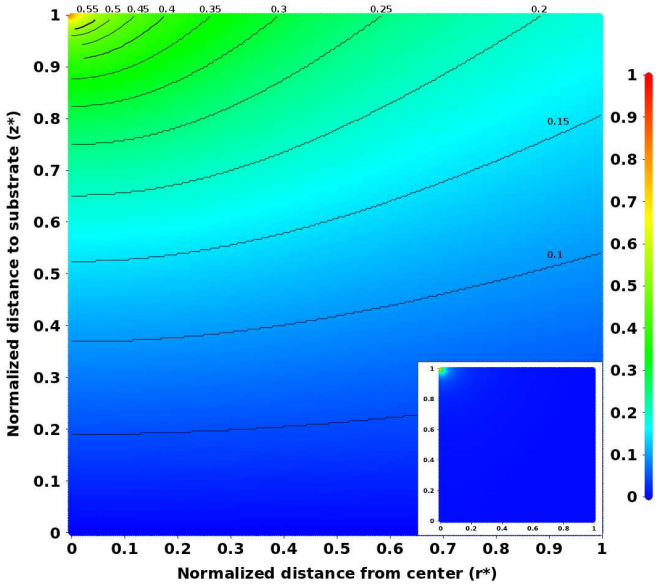

Fig. 5. Magnitude of the normalized electric potential Φ/Φ_0 during ESD processing. The distance between needle and deposition plate as well as the radial distance from the center are normalized to the distance between the atomizer and the substrate. The inset is the normalized electric field distribution.

It is clear that the effects of K_V should be included in the droplet transport model when $R/H > 0.005$.

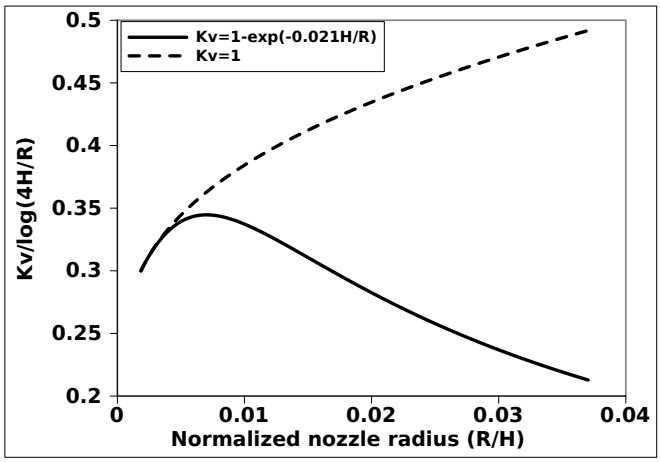

Fig. 6. The effects of varying the atomizing nozzle's outer radius on the strength of the electric field with and without the K_V effects.

The droplet displacement resulting from the acceleration given in (10) is given by

$$d_v\left(t\right) = C_1 e^{-r_1 t} + C_2 e^{-r_2 t} + C_3, \tag{13}$$

where

$$r_1 = \frac{-s + \sqrt{s^2 - 4\,c_v}}{2}, \quad r_2 = \frac{-s - \sqrt{s^2 - 4\,c_v}}{2}, \tag{14}$$

and

$$C_1 = r_1 v_{v0} - \frac{r_1^2\,r_2}{r_1 - r_2}\left[(g-l) - v_{v0}\left(\frac{1}{r_1} + s\right)\right],$$
$$C_2 = \frac{r_1\,r_2^2}{r_1 - r_2}\left[(g-l) - v_{v0}\left(\frac{1}{r_1} + s\right)\right], \tag{15}$$
$$C_3 = \frac{c_v}{1 + (g-l) + s}.$$

ISBN: 978-988-19252-8-2
ISSN: 2078-0958 (Print); ISSN: 2078-0966 (Online)

An explicit equation for the time required to achieve the displacement in (13) cannot be found. Therefore, the droplet motion is solved by time discretization, MC methods, or iteratively in order to obtain the droplet trajectory through the electric field. An iterative solver is implemented within the simulator, which solves the Lambert function, appearing after inverting (13) [19].

After finding the time required for the droplet to reach the height of the wafer surface, a similar derivation can be used to find the radial location of the droplet using the vertical flight time.

B. Modeling Interaction between Droplet and Wafer Surface

There are two main types of depositions which have been examined. One type relies on the droplets being transported very near the surface, where they undergo evaporation and the resulting vapor causes a CVD-like deposition process on the silicon surface. The other type relies on the droplet reaching the surface before it is fully evaporated and sticking on the silicon wafer while simultaneously spreading. The former is commonly the result of a PSD deposition process, while the latter is common for ESD processes, where the droplets are accelerated at much higher speeds and therefore have enough force to overcome the retardant Stokes and thermophoretic forces to reach the substrate as a liquid.

IV. Spray Pyrolysis Deposition Simulations

A. YSZ Deposition using ESD Pyrolysis

The YSZ deposition using an ESD process from [11] is simulated using the model discussed in the previous section. The first step is finding the droplet size as it exits the atomizer. The distribution of droplet sizes does not follow any standard distribution, but it is suggested that the volume fraction varies relatively evenly near the approximate value 0.05 for droplets between with a radius between $2.5\mu m$ and $55\mu m$ [11], [20]. Therefore, the distribution for the droplet radii is simulated by generating an even distribution for the volume fraction ξ_{vol} followed by finding the radius distribution for the droplet r_d:

$$r_d = \left\{ \xi \cdot \left[(r_+)^{-1/3} - (r_-)^{-1/3} \right] + (r_-)^{-1/3} \right\}^{-3}, \quad (16)$$

where $r_- = 2.5\mu m$ and $r_+ = 55\mu m$ are the minimum and maximum radii for the generated droplets and $\xi \in [0, 1]$ is an evenly distributed random value.

The given equation for the electric field provides the magnitude at each location; however, in order to follow the droplet trajectory, the individual components of the electric field in each direction are required such that, in cylindrical coordinates, $\vec{E}_{ext} = (E_\rho, \varphi, E_z)$. The droplet angle φ is unaffected by the applied forces since they act only in the radial ρ and vertical z directions.

Fig. 7 shows an area which expands 250μm by 250μm. Several droplets are shown including overlapping of the disk shapes on the surface as they are being deposited. The lighter surface is silicon while the darker disks are the deposited YSZ films. Each depositing droplet is modeled using 10^9 particles which accelerate to the surface and add a slight component of the overall deposited film thickness.

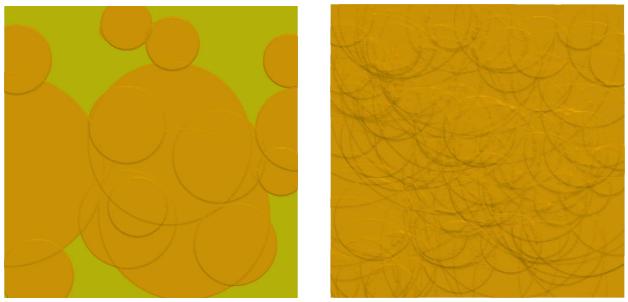

(a) 15 droplets (b) 100 droplets

Fig. 7. Spray pyrolysis simulation on a 250μm by 250μm geometry.

B. Tin Oxide Deposition using PSD Pyrolysis

The deposition of tin oxide (SnO_2) on silicon dioxide using the spray pyrolysis deposition process was performed using an air atomizer which is not located directly above the wafer, but rather on the side, emitting a spray towards the wafer. The nitrogen pressure of the atomizer was set to 2bar in air and 0.7bar in the liquid. These values are outside of the data sheet for the nozzle used [13], which is done in order to obtain smaller droplet sizes and slower deposition rates [2]. However, the data sheet information was extracted and the provided graph extended in order to find an approximate radial distribution of particles. The droplet radii vary between 1.5μm and 5.5μm. The spray direction is also extrapolated from the data sheet for the simulation. The spray nozzle in use is one which produces a flat spray pattern with droplet dispersal proceeding mainly in the lateral axial direction. The nozzle is approximately 20cm laterally and 10cm vertically distanced from the substrate and the spray is directed such that much of it is found above the heated surface, where it can deposit onto the wafer.

In the ESD system, the flight of individual droplets was modeled in order to analyze the film deposition. However, in the PSD system, due to the lack of a strong electrical force, it is clear that the droplets cannot be viewed individually, but that interactions between droplets during their flight plays a significant role in their trajectory. Droplets move through air as a flux and calculating individual droplet's movements in order to find their final location on the wafer surface does not produce a match to the experimental results, shown in Fig. 8 (a).

There are several factors which influence the final thickness of the deposited film. Those include the spraying time, volume of the sprayed solution, air pressure, distance of the atomizer from the substrate, temperature of the pyrolysis reaction, and time of the solution ($SnCl_4$) aging. It was found in [7] that thicknesses of the deposited SnO_2 film decrease, when the time interval between its preparation and its use in the pyrolysis reaction increases. A suggestion is made to use either a freshly made solution or a completely aged solution during spray pyrolysis. During the presented experiments, the the nozzle distance to the substrate, air pressure, and solution aging remain constant, while the spray is constantly applied. The nozzle's distance to the substrate is set to 20cm laterally and 10cm vertically, the air pressure to 1atm, and the solution is freshly prepared. In correspondence, the time and temperature dependences are investigated in the model.

Our experimental data suggest a linear dependence on

ISBN: 978-988-19252-8-2
ISSN: 2078-0958 (Print); ISSN: 2078-0966 (Online)

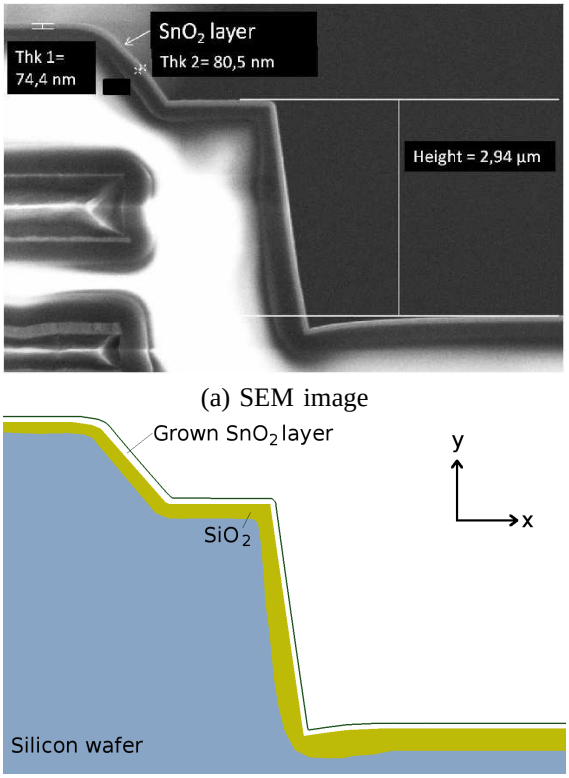

(a) SEM image

(b) Simulation

Fig. 8. Images showing the deposited SnO_2 film as a results of a PSD deposition step. The good step coverage confirms a chemical and not physical reaction takes place during deposition.

spray time and a logarithmic dependence on wafer temperature for the growth rate of the deposited SnO_2 layer. A good agreement is given by the Arrhenius expression

$$d_{SnO_2}(t,T) = A_1\, t\, e^{(-E/k_B T)}, \qquad (17)$$

where $A_1 = 3.1\,\mu m/s$, the thickness is given in μm, t is the time in seconds, T is the temperature in Kelvin, and E is $0.427eV$. Fig. 8 depicts the (a) experimental and (b) simulated topography of a deposited SnO_2 film on a step structure after applying a PSD process for 45 seconds at 400°C. The incoming flux is set to flow in the (x, y) = (-0.32,-0.95) direction and a CVD-like process is simulated with a reaction order of 1 and a sticking probability of 0.2, producing a good fit to the experimental data. The average direction of the initial flow is (-1,0), but due to the effects of gravity in the vertical direction, the droplet flux experiences a downward acceleration. However, in the lateral motion, it only experiences the retardant Stokes force. Therefore, it is evident that the direction of the flux will change from mainly horizontal to mainly vertical as it reaches the wafer.

V. Conclusion

In order to manufacture smart gas sensor devices, the spray pyrolysis deposition technique is used to grow an ultrathin SnO_2 layer. The thin film reacts with the gas at high temperatures to allow for charge transfer between the gas and surface, modifying the electrical conductance in the process. The spray pyrolysis technique is found to be cost effective and is seamlessly integrated in a series of CMOS processing steps. A model for spray pyrolysis deposition has been presented and integrated into a topography process simulator using the Level Set method. The model examines the changing topography, when multiple droplets undergo trajectories dictated by the applied forces, finally striking the surface for deposition. In addition, a model similar to CVD deposition is suggested, when the droplets can be seen as a flux and not as individual particles and when they evaporate near the surface prior to fully contacting the wafer in liquid form.

References

[1] G. L. Messing, S.-C. Zhang, and G. V. Jayanthi, "Ceramic powder synthesis by spray pyrolysis," *Journal of the American Ceramic Society*, vol. 76, no. 11, pp. 2707–2726, 1993.

[2] A. Tischner, T. Maier, C. Stepper, and A. Köck, "Ultrathin SnO_2 gas sensors fabricated by spray pyrolysis for the detection of humidity and carbon monoxide," *Sensors and Actuators B: Chemical*, vol. 134, no. 2, pp. 796–802, 2008.

[3] G. Mutinati, E. Brunet, S. Steinhauer, A. Köck, J. Teva, J. Kraft, J. Siegert, F. Schrank, and E. Bertagnolli, "CMOS-integrable ultrathin SnO_2 layer for smart gas sensor devices," *Procedia Engineering*, vol. 47, 2012.

[4] O. Ertl, "Numerical methods for topography simulation," Dissertation, Technischen Universität Wien, Fakultät für Elektrotechnik und Informationstechnik, May 2010, http://www.iue.tuwien.ac.at/phd/ertl/.

[5] A. Nakaruk and C. Sorrell, "Conceptual model for spray pyrolysis mechanism: fabrication and annealing of titania thin films," *Journal of Coatings Technology and Research*, vol. 7, no. 5, pp. 665–676, 2010.

[6] S. Major, A. Banerjee, and K. Chopra, "Highly transparent and conducting indium-doped zinc oxide films by spray pyrolysis," *Thin Solid Films*, vol. 108, no. 3, pp. 333–340, 1983.

[7] G. Korotcenkov, V. Brinzari, J. Schwank, M. DiBattista, and A. Vasiliev, "Peculiarities of SnO_2 thin film deposition by spray pyrolysis for gas sensor application," *Sensors and Actuators B: Chemical*, vol. 77, no. 1–2, pp. 244–252, 2001.

[8] D. Perednis and L. J. Gauckler, "Solid oxide fuel cells with electrolytes prepared via spray pyrolysis," *Solid State Ionics*, vol. 166, no. 3-4, pp. 229–239, 2004.

[9] S. H. Ng, J. Wang, D. Wexler, S. Y. Chew, and H. K. Liu, "Amorphous carbon-coated silicon nanocomposites: a low-temperature synthesis via spray pyrolysis and their application as high-capacity anodes for lithium-ion batteries," *The Journal of Physical Chemistry C*, vol. 111, no. 29, pp. 11 131–11 138, 2007.

[10] G. Blandenet, M. Court, and Y. Lagarde, "Thin layers deposited by the pyrosol process," *Thin Solid Films*, vol. 77, no. 1–3, pp. 81–90, 1981.

[11] D. Perednis, "Thin film deposition by spray pyrolysis and the application in solid oxide fuel cells," Dissertation, Eidgenössische Technische Hochschule (ETH) Zürich, 2003, http://e-collection.library.ethz.ch/eserv/eth:26881/eth-26881-02.pdf.

[12] A. J. Kelly, "Charge injection electrostatic atomizer modeling," *Aerosol Science and Technology*, vol. 12, no. 3, pp. 526–537, 1990.

[13] "Spraying Systems Co., Volume median diameter versus air pressure at constant liquid pressures," data Sheet No. 36892-8M.

[14] J. C. Viguié and J. Spitz, "Chemical vapor deposition at low temperatures," *Journal of The Electrochemical Society*, vol. 122, no. 4, pp. 585–588, 1975.

[15] W. Siefert, "Properties of thin In_2O_3 and SnO_2 films prepared by corona spray pyrolysis, and a discussion of the spray pyrolysis process," *Thin Solid Films*, vol. 120, no. 4, pp. 275–282, 1984.

[16] I. W. Lenggoro, "An experimental and modeling investigation of particle production by spray pyrolysis using a laminar flow aerosol reactor," *Journal of Materials Research*, vol. 15, no. 3, pp. 733–743, 2000.

[17] L. Filipovic, "Topography simulation of novel processing techniques," Dissertation, Technischen Universität Wien, Fakultät für Elektrotechnik und Informationstechnik, December 2012, http://www.iue.tuwien.ac.at/phd/filipovic/.

[18] A. Gañán-Calvo, J. Lasheras, J. Dávila, and A. Barrero, "The electrostatic spray emitted from an electrified conical meniscus," *Journal of Aerosol Science*, vol. 25, no. 6, pp. 1121–1142, 1994.

[19] D. Veberic, "Having Fun with Lambert W(x) Function," *ArXiv e-prints*, Mar. 2010, http://adsabs.harvard.edu/abs/2010arXiv1003.1628V.

[20] O. Wilhelm, "Electrohydrodynamic spraying – transport, mass and heat transfer of charged droplets and their application to the deposition of thin functional films." Dissertation, Swiss Federal Institute of Technology Zurich - Eidgenössische Technische Hochschule (ETH) Zürich, 2004, http://fex-dev2.ethz.ch/eserv/eth:27191/eth-27191-02.pdf.

ISBN: 978-988-19252-8-2
ISSN: 2078-0958 (Print); ISSN: 2078-0966 (Online)